



**HAL**  
open science

## **Amplified Fluorescence in Situ Hybridization by Small and Bright Dye-Loaded Polymeric Nanoparticles**

Sylvie Egloff, Nina Melnychuk, Elisabete Cruz da Silva, Andreas Reisch, Sophie Martin, Andrey S Klymchenko

► **To cite this version:**

Sylvie Egloff, Nina Melnychuk, Elisabete Cruz da Silva, Andreas Reisch, Sophie Martin, et al.. Amplified Fluorescence in Situ Hybridization by Small and Bright Dye-Loaded Polymeric Nanoparticles. *ACS Nano*, 2021, 16 (1), pp.1381-1394. <10.1021/acsnano.1c09409>. <hal-03573138>

**HAL Id: hal-03573138**

**<https://hal.science/hal-03573138v1>**

Submitted on 14 Feb 2022

**HAL** is a multi-disciplinary open access archive for the deposit and dissemination of scientific research documents, whether they are published or not. The documents may come from teaching and research institutions in France or abroad, or from public or private research centers.

L'archive ouverte pluridisciplinaire **HAL**, est destinée au dépôt et à la diffusion de documents scientifiques de niveau recherche, publiés ou non, émanant des établissements d'enseignement et de recherche français ou étrangers, des laboratoires publics ou privés.



HAL Authorization

# Amplified Fluorescence *in Situ* Hybridization by Small and Bright Dye-Loaded Polymeric Nanoparticles

Sylvie Egloff,<sup>§</sup> Nina Melnychuk,<sup>§</sup> Elisabete Cruz Da Silva, Andreas Reisch, Sophie Martin, Andrey S. Klymchenko\*

Laboratoire de Bioimagerie et Pathologies, UMR 7021 CNRS, Faculté de Pharmacie, Université de Strasbourg, 74, Route du Rhin, 67401 Illkirch, France.

<sup>§</sup> These authors contributed equally to this work.

\*Corresponding author. E-mail address: andrey.klymchenko@unistra.fr (A. S. Klymchenko); tel: +33 368 85 42 55.

## Abstract

Detection and imaging of RNA at the single-cell level is of utmost importance for fundamental research and clinical diagnostics. Current techniques of RNA analysis, including fluorescence *in situ* hybridization (FISH), are long, complex and expensive. Here, we report a methodology of amplified FISH (AmpliFISH) that enables simpler and faster RNA imaging using small and ultrabright dye-loaded polymeric nanoparticles (NPs) functionalized with DNA. We found that the small size of NPs (below 20 nm) was essential for their access to the intracellular mRNA targets in fixed permeabilized cells. Moreover, proper selection of the polymer matrix of DNA-NPs minimized nonspecific intracellular interactions. Optimized DNA-NPs enabled sequence-specific imaging of different mRNA targets (survivin, actin and polyA tails), using a simple 1h staining protocol. Encapsulation of cyanine and rhodamine dyes with bulky counterions yielded green, red and far-red emitting NPs that were 2-100-fold brighter than corresponding quantum dots. These NPs enabled multiplexed detection of three mRNA targets simultaneously, showing distinctive mRNA expression profiles in three cancer cell lines. Image analysis confirmed the single-particle nature of the intracellular signal, suggesting single-molecule sensitivity of the method. AmpliFISH was found to be semi-quantitative, correlating with RT-qPCR. In comparison with the commercial LNA-based FISH technique, AmpliFISH provides 8-200-fold stronger signal (dependent on the NP color) and requires only 3 steps vs. ~20 steps together with much shorter time. Thus, combination of bright fluorescent polymeric NPs with FISH yields a fast and sensitive single-cell transcriptomic analysis method for RNA research and clinical diagnostics.

**Keywords:** fluorescent nanoparticles; DNA-functionalized polymeric nanoparticles; fluorescence *in situ* hybridization; single-cell analysis; RNA imaging; mRNA; fluorescence microscopy.

With the ever growing role of RNA in understanding and controlling cellular processes,<sup>1,2</sup> detection and imaging of intracellular RNA attract significant attention.<sup>3-5</sup> Current approaches include fluorescence situ hybridization (FISH),<sup>6</sup> single-cell RNA-sequencing,<sup>7,8</sup> as well as molecular biology techniques based on labelled RNA-binding proteins<sup>4,9</sup> and light-up aptamers.<sup>10-14</sup> *In situ* hybridization, introduced more than 50 years ago,<sup>15,16</sup> and its fluorescence version FISH<sup>17,18</sup> are particularly suitable for imaging native nucleic acids within cells and tissues, with applications ranging from fundamental RNA research to clinical diagnostics.<sup>6,19</sup> In particular, RNA-FISH, which allows spatial and temporal monitoring of intracellular RNA provides important insights into mechanisms of transcription and translation<sup>20,21</sup> and serve as tool for cell-based diagnostics.<sup>22,23</sup> Advanced versions of RNA-FISH, developed in the last decades, enable detection and quantification of intracellular RNA with single molecule sensitivity.<sup>24-27</sup> Nevertheless, broad applications of RNA-FISH in research and clinical diagnostics are still limited by a number of challenges. In particular, low-abundant RNA are still difficult to identify,<sup>28</sup> because of limited fluorescence signal provided by single organic dye molecules. Therefore, many approaches have been developed to amplify the fluorescence signal, such as branched DNA amplification,<sup>29-31</sup> different isothermal amplification strategies,<sup>32</sup> rolling circle amplification (RPA),<sup>33</sup> hybridization chain reaction (HCR),<sup>34,35</sup> primer-exchange reaction,<sup>36,37</sup> and click-amplifying FISH (ClampFISH).<sup>38</sup> The signal amplification can be also achieved by using multiple singly labeled oligonucleotides (generally 30–48) that hybridize along the same target RNA transcript,<sup>27</sup> known as Stellaris™ FISH method.<sup>39</sup> However, FISH techniques include complicated time-consuming procedures with multiple steps and require experienced staff, which make development of validated protocols for clinics very expensive.<sup>40</sup> Moreover, FISH protocols are probe- and sample-dependent and have to be optimized for each set of conditions.<sup>41</sup>

Fluorescent probes based on nanoparticles (NPs) can potentially overcome some of the limitations in the field of nucleic acid detection.<sup>42</sup> In particular, high fluorescence brightness of NPs may allow direct detection of the biomolecular targets without the need of complex and time-consuming amplification protocols.<sup>43-48</sup> NPs can provide fluorescence signal amplification for nucleic acid detection using different mechanisms, including energy transfer from semiconductor quantum dots<sup>49</sup> and polymeric NPs<sup>50-52</sup> as well as plasmonics-based fluorescence enhancement,<sup>53,54</sup> hybridization-triggered molecular assembly,<sup>55</sup> *etc.* Direct intracellular detection of nucleic acids by NPs inside the cells is a highly attractive approach,<sup>56</sup> and a few reported examples include gold nanoparticles (nano-flares)<sup>57-59</sup> DNA-based nanostructures,<sup>60-63</sup> semiconductor quantum dots,<sup>64,65</sup> upconversion NPs,<sup>66</sup> carbon nanostructures,<sup>67,68</sup> as well as lipid NPs,<sup>69,70</sup> polymeric NPs,<sup>71</sup> hybrid organic-inorganic NPs,<sup>72</sup> *etc.* However, RNA detection in live cells remains complicated by efficient endocytosis of nanomaterials with their potential degradation by enzymes and generic problem of endosomal escape of entrapped NPs.<sup>73-75</sup> In this respect, combination of FISH technique in fixed and permeabilized cells with luminescent NPs is of particular interest, because it can ensure direct access of NPs to the target RNA and take advantage of established FISH protocols in biological and clinical applications.<sup>19</sup> However, this possibility was realized only recently using semiconductor quantum dots (QDs) in combination with Stellaris™ approach, where distinct mRNA transcripts have been detected and quantified at the single-molecule level in individual cells.<sup>65</sup> To achieve this, the authors specially designed compact QDs, which could access better the whole cytosol and thus hybridize with the intracellular mRNA.<sup>65</sup>

Dye-loaded polymeric nanoparticles, which attracted attention in the recent years due to their high brightness and modularity,<sup>45,76</sup> could be a promising platform for development of a simple and rapid

RNA-FISH probes. To address a problem of aggregation-caused quenching of encapsulated dyes in these NPs, we proposed a concept of ionic dye insulation by bulky hydrophobic counterions, yielding NPs 6-100 fold brighter than corresponding QDs.<sup>52,77,78</sup> The size of these NPs can be tuned from 10 to 50 nm depending on the nature of the polymer,<sup>79</sup> which is a critical point because NPs should be able to reach the RNA target within the cytosol.<sup>65</sup> Indeed, polymeric NPs with sizes < 23 nm are required to diffuse and spread in the cytosol of living cells.<sup>80</sup> In addition to rhodamine dye, cyanine dyes can also be encapsulated to prepare NPs of any desired color, which was applied for multi-color barcoding of live cells and for long term tracking *in vitro* and *in vivo*.<sup>81</sup> Moreover, the efficient energy transfer within donor dyes inside the NPs can generate a giant light-harvesting antenna that amplifies the fluorescence signal of a single acceptor >1000-fold.<sup>82</sup> Their functionalization with oligonucleotides yielded nanoprobe for amplified detection of DNA and RNA in solutions with picomolar limit of detection<sup>52</sup> and on surfaces with single-molecule sensitivity<sup>51</sup> and compatibility with mobile phone camera.<sup>83</sup> These DNA-functionalized NPs have already been validated for detection of microRNA in cell extracts,<sup>84</sup> but they have not been explored to date for direct detection of RNA inside the cells.

In the present work, we developed a methodology of amplified FISH (AmpliFISH) based on ultrabright dye-loaded polymeric NPs functionalized with DNA. In this approach, the hybridization AmpliFISH probe with the target mRNA inside the cells results in the fluorescence signal equivalent to 80-300 encapsulated dyes per single sequence, which ensures strong signal amplification. We show that the size of NPs <16 nm was essential to achieve effective penetration of fixed cells and hybridization with the target. Owing to their high brightness, these FISH nanoprobe can detect target mRNA in fixed cells using a simple and rapid protocol (< 3h). Importantly, FISH nanoprobe of three different colors could be used simultaneously to target different RNA sequences. The methodology was validated on three cancer cell lines and it allows semi-quantitative analysis of mRNA abundance. The developed probes and the FISH methodology can greatly simplify FISH based imaging of RNA inside cells for both fundamental research and clinical diagnostics.

## Results and discussion

**Design and optimization of FISH nanoprobe.** The design of our FISH nanoprobe is based on dye-loaded polymeric NPs functionalized with nucleic acids complementary to the mRNA target (Figure 1). Dye-loaded NPs are made of poly(methyl methacrylate) (PMMA) or poly(ethyl methacrylate) (PEMA) polymers bearing azide and negatively charged carboxylate group (Figure 1A). Nanoprecipitation of these hydrophobic polymers with charged groups yields ultrasmall NPs, where the core is formed by the hydrophobic domain of the polymer, while the charged carboxylate exposes azide group at the NP surface to ensure high reactivity for the click reaction.<sup>51,52,85</sup> For encapsulation, we used octadecyl rhodamine B R18 with its bulky hydrophobic counterion trakis(pentafluorophenyl)borate (F5). The latter serves as insulator that prevents the dyes from aggregation-caused quenching when loaded at high concentration and at the same time ensure effective encapsulation without dye leakage.<sup>77,86</sup> The dye-loaded NPs were obtained by nanoprecipitation of the polymer and the dye from acetonitrile into corresponding buffer. Then, oligonucleotides were grafted to the NPs surface by reacting the exposed azide groups with DBCO groups of oligonucleotides (Figure 1A). The sequence of grafted oligonucleotides was a 20-22mers complementary to the target mRNA of actin and survivin. The former is a common housekeeping gene well expressed in many cell lines, while the latter is a common marker of cancer cells.<sup>87</sup> In our



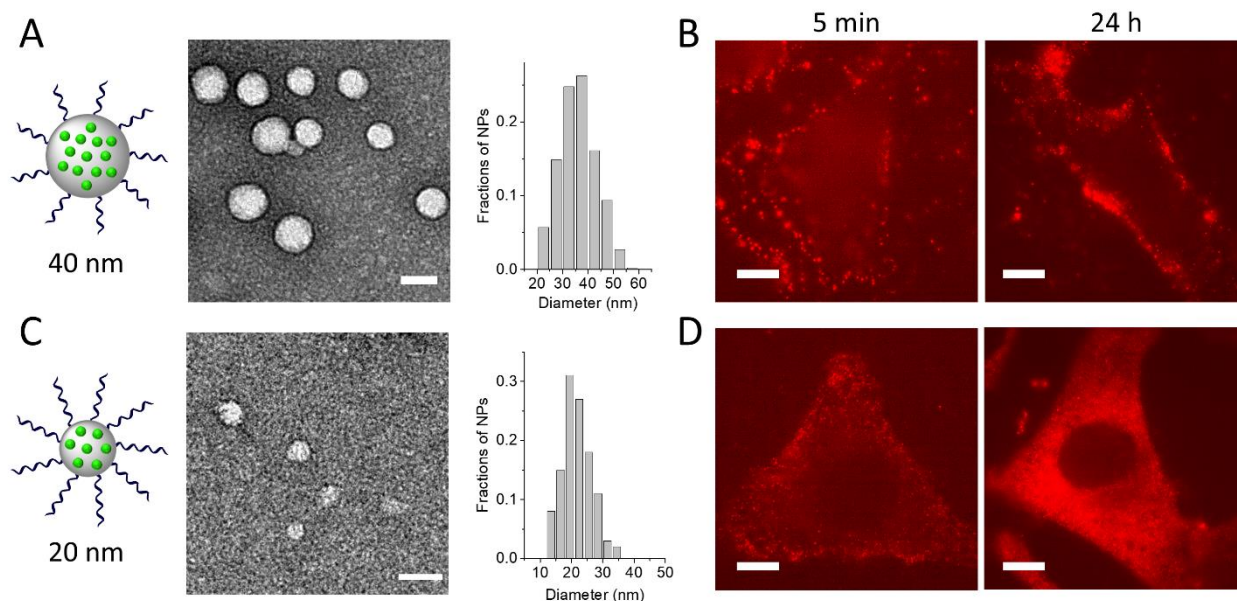


**Figure 2.** Testing DNA-functionalized NPs of two different sizes in fixed permeabilized HeLa cells. (A, C) NPs of two different average sizes of their core,  $\sim 40$  nm (A) and  $\sim 20$  nm (C) and their corresponding TEM images and size distribution histograms. (B, D) Fluorescence microscopy (TIRF) images of cells labelled for different time (5 min and 24 h) with DNA-NPs (T20-NPs) of two different sizes:  $\sim 40$  nm (B) and  $\sim 20$  nm (D). Scale bar is  $10 \mu\text{m}$ .

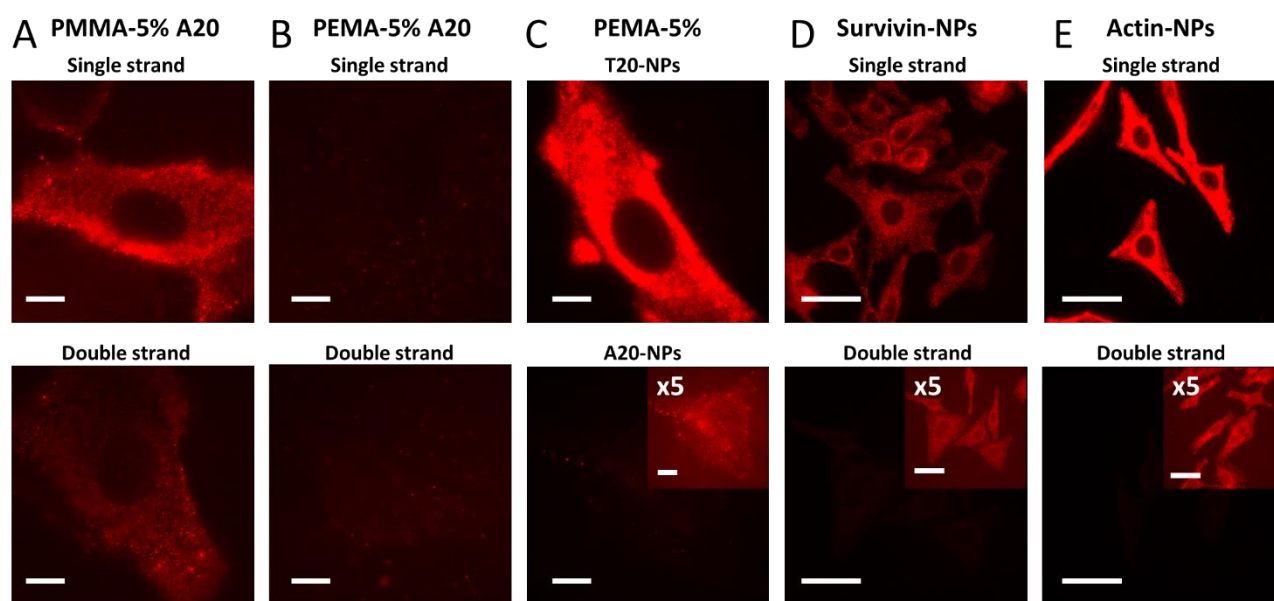


**Figure 3.** Effect of polymer nature and different grafted DNA sequences. (A, B) Fluorescence images of fixed HeLa cells incubated with PMMA-based NPs (A) and PEMA-based NPs (B) of  $\sim 20$  nm core size, functionalized with A20. Both single-stranded and double-stranded (annealed with T20) DNA NPs were tested (30 min incubation with cells). TIRF mode was used on fixed HeLa cells without washing. (C) Comparison of TIRF fluorescence images of PEMA-based NPs functionalized with T20 (upper panel) and A20 (lower panel) recorded at identical conditions (inset shows an image where signal was amplified 5-fold for visibility of the cell). Cells were incubated during 1 h with NPs, then washed two times with 0.1 % BSA / PBS. Scale bar:  $10 \mu\text{m}$ . (D, E) Epi-fluorescence microscopy of fixed HeLa cells incubated for 1 h with DNA-NPs targeting survivin and  $\beta$ -actin (the same washing

protocol as in C). Images for single-stranded (upper panels) and double-stranded (annealed with complementary strands) DNA-NPs are shown. Scale bar: 50  $\mu$ m. PBS buffer with 50 mg / L Tween 80 was systematically used for incubation and imaging (A-E).

Then, we tested whether the hybridization with the poly(A) tails is specific. We replaced T20 DNA with A20 DNA, which is not expected to hybridize with the poly(A) targets. However, microscopy experiments showed that the intracellular signal for these NPs remained high, indicating strong non-specific interactions of NPs inside the cells (Figure 3A). We further annealed the A20-functionalized NPs with T20 DNA to obtain double stranded oligonucleotides at the NPs surface. In this case, the intracellular signal decreased (Figure 3A, S1), but still remained significant, confirming the non-specific interactions of NPs with the cells, independent from the DNA/RNA hybridization. Therefore, we formulated small NPs based on another polymer, PEMA bearing 5% charged groups (PEMA-MA-5%), which was previously shown to yield  $\sim$ 20 nm ultrabright NPs.<sup>51</sup> Importantly, the cell experiments revealed practically no signal for A20-functionalized PEMA-based NPs (Figure 3B, S1). Similar low intracellular signal was observed for the NPs bearing A20 annealed with T20 DNA. Then, we directly compared PEMA-based NPs functionalized with A20 DNA (A20-NPs) and T20 DNA (T20-NPs). Strong intracellular signal was observed in case of T20-NPs, while the signal from A20-NPs was very weak and could only be detected when the signal in the image was multiplied 5-fold (Figure 3C, S1). Thus, the use of PEMA-based NPs dramatically decreased non-specific interactions, allowing direct detection of T20-NPs specifically hybridized with poly(A) targets inside the cells. It could be related to narrower size distribution of these PEMA-based NPs (see below), compared to PMMA NPs. The second reason could be more hydrophobic nature of PEMA compared to PMMA (ethyl vs. methyl group), which can provide better stability to DNA-NPs, where the core is formed essentially due to hydrophobic collapse of the polymer. It should be added, that small size of PEMA-based NPs should limit the number of grafted oligonucleotides per particle to  $\sim$ 80, according to our earlier studies on analogous DNA-NPs,<sup>51</sup> which is important to minimize the off-target non-specific interactions.

Then, we functionalized PEMA-based NPs with capture DNA sequences complementary to survivin and  $\beta$ -actin mRNA and tested them in cells. Both nanoprobe showed significant intracellular signal inside the cells (Figure 3D,E, S2), which was significantly higher in case of  $\beta$ -actin (see below). To verify the contribution of non-specific interactions, we annealed our DNA-NPs with complementary short oligonucleotides in solution to block their capacity to hybridize with corresponding intracellular mRNA targets. Importantly, the intracellular signal decreased drastically for the double-stranded nanoprobe, so that 5-fold multiplication of the signal was required to observe some cell fluorescence (Figure 3D, E, S2). These first experiments showed that we could observe sequence-specific hybridization of our DNA-NPs with the intracellular mRNA targets. It should be noted that in all these images, the nucleus remained dark, indicating that NPs could not penetrate through the nuclear envelope.

**DNA-NPs of different color.** Next, we prepared NPs of three different colors in order to perform multi-color detection of target mRNA. In addition to red emitting R18/F5, we selected green rhodamine 110 derivative with octadecyl chain (Rh110-C18)<sup>83</sup> and far red cyanine DiD (Figure 4). As a counterion for these two dyes, we used the bulkiest available counterion F12, which was shown previously to ensure the highest fluorescence quantum yields (QY) for the NPs.<sup>81,83</sup> We formulated bare NPs loaded with corresponding dyes and checked the QY at different dye loading. For all three

dyes, QY decreased with increase in the high loading (Table S1), indicating some effect of dye self-quenching. Based on these data, we could choose optimal high loading, where QY remained significantly high: 30 wt% for all three dye salts, with quantum yields of 52, 34 and 42% for R18/F5, R110-C18/F12 and DiD/F12. The size of the obtained bare NPs at 30 wt% dye loading remained small according to DLS (~17 nm) and TEM (14-18 nm, Table S2). TEM imaging confirmed the spherical shape of bare NPs (Figure 5). Then, we functionalized them with A20 or T20, using the same protocol based on SPAAC reaction. The QY values did not change after functionalization and thus remained relatively high. The absorption and fluorescence spectra of DNA-NPs showed well defined and well separated bands (Figure 4), typical for the molecular forms of these three dyes. These bands match well common optical settings of the microscope in the green, red and far-red channels. According to TEM of DNA-NPs, the size of the spherically-shaped particles did not significantly change, since only ~2 nm increase was observed after functionalization (Figure 5, Table S2). It is important to note that relatively narrow size distribution of all these DNA-NPs, so that all detected NPs were systematically <25 nm. This is a key difference with PMMA-based NPs, where for similar particle size, NPs >30 nm were still observed (Figure 2C). This narrower size distribution could explain why PEMA-based NPs showed much less non-specific interactions (or NPs trapping) inside the cells (see above, Figure 3). On the other hand, DLS data suggested that after DNA-functionalization, the particle size increased by 6-7 nm (Table S2), which corresponds to the lengths of two 20mer strands grafted to the NP surface. In contrast to TEM, DLS records the hydrodynamic diameter that takes into account the relatively thick hydration shell formed by grafted nucleic acids.

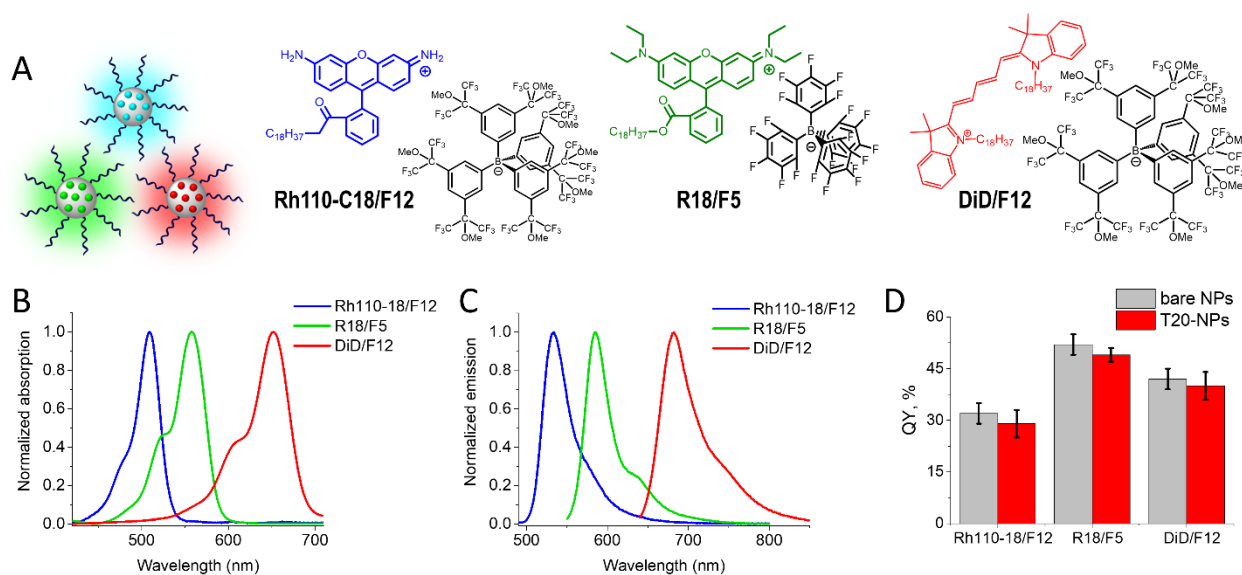


**Figure 4.** FISH-NPs of three different colors. (A) Dye salts with bulky counterions used for encapsulation into polymeric NPs. (B) Absorption and (C) Fluorescence spectra of DNA-NPs loading three different dye salts. (D) Fluorescence quantum yields of bare NPs and DNA-NPs (T20 oligonucleotide). Dye loading (weight% ratio with respect to the polymer) was 30 wt%. Error bars are standard deviation ( $n \geq 3$ ).

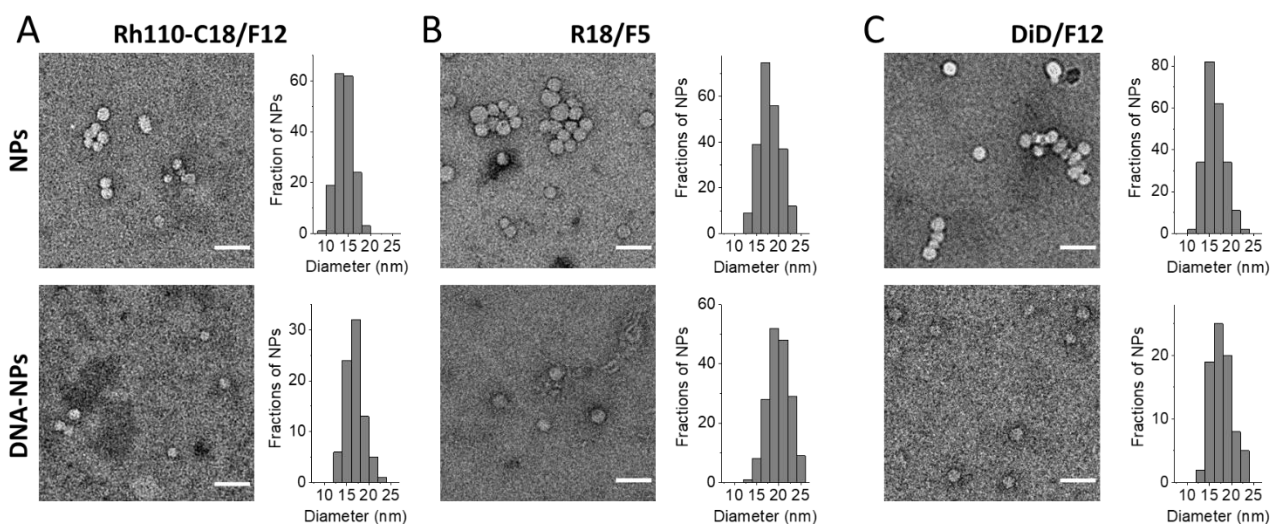


**Figure 5.** TEM characterization of DNA-NPs of different color functionalized with T20 oligonucleotides. TEM images of DNA-NPs loaded at 30 wt% with Rh110-18/F12 (A), R18/R5-TPB (B), and DiD/F12 (C) and corresponding size distribution histograms at the right (at least 200 NPs were analyzed per condition). Upper panels correspond to bare NPs, while lower panels correspond to DNA-NPs.

Then, we characterized the obtained DNA-NPs at the single particle level using wide-field fluorescence microscopy. For each color of NPs, we made a comparison with corresponding QDs characterized by similar emission wavelength. All studied DNA-NPs, which appeared as dots in the microscopy images, were significantly brighter than corresponding QDs (Figure 6). Quantitative analysis of the single particle brightness revealed that green, red and far-red DNA-NPs were  $2.3 \pm 0.8$ ,  $97 \pm 6$  and  $16 \pm 2$ -fold brighter than corresponding QDs (Figure 6). These differences correspond to the theoretical brightness (B) of our NPs, which can be expressed as  $B = N \times \epsilon \times QY / 100$ , where N is the number of dyes per NP,  $\epsilon$  is the absorption coefficient ( $M^{-1}cm^{-1}$ ) at the excitation wavelength used and QY is the fluorescence quantum yield (%) of the dye inside the NP. Taking the average NP size of bare NPs loaded with Rh110-18/F12, R18/R5-TPB, and DiD/F12 NPs 14, 18 and 16 nm, respectively, according to TEM, and 30 wt% loading of the dyes vs. polymer (*i.e.* 23% vs. total particle mass), the corresponding estimated N is 85, 308, 113. Then, the estimated single particle brightness is  $6.9 \times 10^5$ ,  $1.8 \times 10^7$  and  $9.7 \times 10^6 M^{-1} \times cm^{-1}$  for Rh110-18/F12, R18/R5-TPB, and DiD/F12 NPs. For QDs QDs-525, QDs-605 and QDs-705, the measured QY values were 77, 52, 49%, respectively. Therefore, their corresponding estimated brightness was  $1.3 \times 10^5$ ,  $3.0 \times 10^5$  and  $4.4 \times 10^5 M^{-1} \times cm^{-1}$  for excitation at 470, 550 and 640 nm, respectively. Thus, theoretically, Rh110-18/F12, R18/R5-TPB, and DiD/F12 should be 5.3, 60 and 22-fold brighter than QDs-525, QDs-605 and QDs-705, respectively, which is close to the obtained experimental values. We should note that these differences would be smaller if QDs were excited at the violet region, where their absorption coefficient is higher. The green DNA-NPs were significantly less bright than other two DNA-NPs because of lower absorption coefficient at the excitation wavelength used (470 nm of LED), lower QY of this dye and less optimal emission filter settings. Overall, we obtained DNA-NPs of similar small size and high brightness, which can be used for multi-color RNA-FISH experiments.

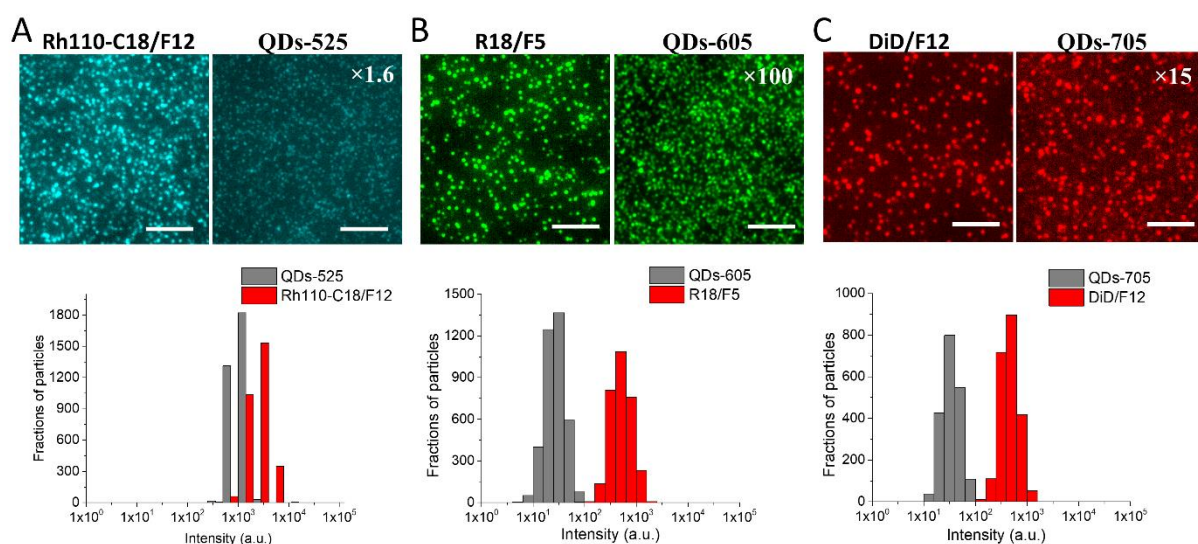


**Figure 6.** Single-particle characterization of DNA-NPs bearing T20 oligonucleotide in comparison to corresponding QDs on glass surface using epi-fluorescence microscopy. Upper panels: fluorescence images of DNA-NPs loaded at 30 wt% with Rh110-C18/F12 vs. QDs-525 (A), R18/R5-TPB vs. QDs-605 (B), and DiD/F12 vs. QDs-705. The signal in QDs was multiplied 1.6- (A) 100- (B) and 15-fold (C) by corresponding increase in the source power for better comparison with brighter DNA-NPs. Scale bar: 5  $\mu$ m. Lower panels: corresponding intensity distribution histograms for DNA-NPs vs. QDs.

**Multicolor detection of mRNA.** We functionalized NPs of three different colors with three capture sequences targeting poly(A),  $\beta$ -actin and survivin fragments of mRNA. After incubation of DNA-NPs with fixed and permeabilized HeLa cells, we observed corresponding staining in each channel: green for  $\beta$ -actin, red for survivin and blue for poly(A) targets (Figure 7). Then, to verify that the binding is sequence dependent, we annealed each nanoprobe with corresponding complementary DNA oligonucleotide and tested in cells. The obtained double stranded DNA-NPs showed practically no emission inside cells, which confirmed low non-specific interactions between NPs and cells. To provide a more direct control for the sequence specificity of our FISH probes, we treated the fixed and permeabilized cells with a competitive sequence complementary to the target (*i.e.* identical to the capture sequence grafted to NPs), which is expected to block the site of binding of our nanoprobe. Importantly,  $\beta$ -actin competitor turned off the intracellular signal from nanoprobe for  $\beta$ -actin, but did not influence those for survivin or poly(A) (Figure 7). By contrast, competitive sequence encoding survivin blocked binding of survivin nanoprobe, but did not affect those targeting actin or poly(A). These experiments showed that our NPs bind intracellular targets with sequence specificity for NPs of different color. We repeated these experiments for U87 (Figure S3) and MDA-MB-231 (Figure S4) cells and obtained similar results with excellent inhibition for both double stranded version of NPs and the competitors for the  $\beta$ -actin and survivin mRNA targets. Thus, the approach works for multiple cell lines.

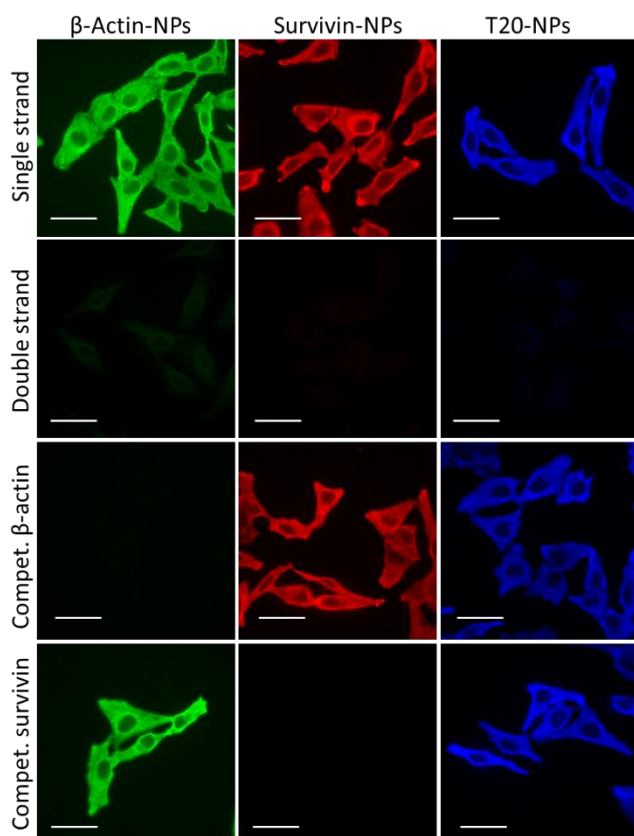


**Figure 7.** Validation of DNA-NPs for detection of intracellular mRNA targets in fixed HeLa cells. Single stranded probes  $\beta$ -actin-NPs loaded with Rh110-C18/F12, survivin-NPs loaded with R18/F5 and A20-NPs loaded with DiD/F12 for  $\beta$ -actin, survivin and poly(A) sequences of mRNA, were compared to controls with double stranded DNA-NPs (annealed with complementary sequences) and competitor oligonucleotides (100 nM) for corresponding  $\beta$ -actin and survivin sequences added 1 h before addition of DNA NPs. DNA-NPs concentration expressed in encapsulated dyes was 100 nM. Scale bar: 50  $\mu$ m.

The next challenge was to image all three target sequences simultaneously by exploiting three colors of NPs bearing corresponding targeting oligonucleotides. To this end, fixed and permeabilized HeLa, U87 and MDA-MB-231 cells were incubated simultaneously with three NPs of different color and further imaged using three channels of the microscope (Figure 8). Importantly, we could obtain signals for all three nanoprobe within the same cell. Each cell showed a distinctive combination of three colors distributed in space (Figure 8B). The green and red colors, encoding  $\beta$ -actin-NPs and survivin-NPs, respectively, did not really colocalize, which can be seen in the zoomed images. This observation was confirmed by a Manders' colocalization, giving relatively low values for  $\beta$ -actin-NPs in survivin-NPs and vice versa for all three cell lines (with only one exception for MDA-MB-231, Table S3). On the other hand, each of them colocalized with the poly(A) target, which can be seen from dominating magenta and cyan colors of the cells (Figure 8B). Indeed, high Manders' colocalization coefficients for  $\beta$ -actin-NPs in T20-NPs were observed, namely 0.998, 0.998 and 0.935 for HeLa, U87 and MDA-MB-231, respectively (Table S3). Similar high values were observed for survivin. These observations can be explained by the fact that both  $\beta$ -actin and survivin mRNAs are expected to have poly(A). On the other hand T20-NPs colocalized with much lower Manders' with  $\beta$ -actin-NPs and survivin-NPs, which is normal because there are many other mRNA having poly(A) tail. In the perinuclear regions, all three colors appeared colocalized giving white pixels. The latter is

probably because too many particles of different color concentrated within areas below the diffraction limited resolution of the microscope, which produced a colocalization effect, even if these NPs are not bound to the same mRNA target. One could also notice that the distribution of the three colors was slightly different for each studied cell line. Indeed, HeLa cells showed tendency to redistribute colors in a rather homogeneous fashion, while the U87 cells showed magenta colors (*i.e.* survivin and poly(A)) localized at extremities of the cells (Figure 8B). In MDA-MB-231 cells, the signals corresponding to  $\beta$ -actin and survivin appeared in similar areas, including the cell edges, providing characteristic yellow regions (Figure 8B). Thus, combination of three nanoprobe reveals distinctive signatures of mRNA distribution at the single cell level for each cancer cell line.

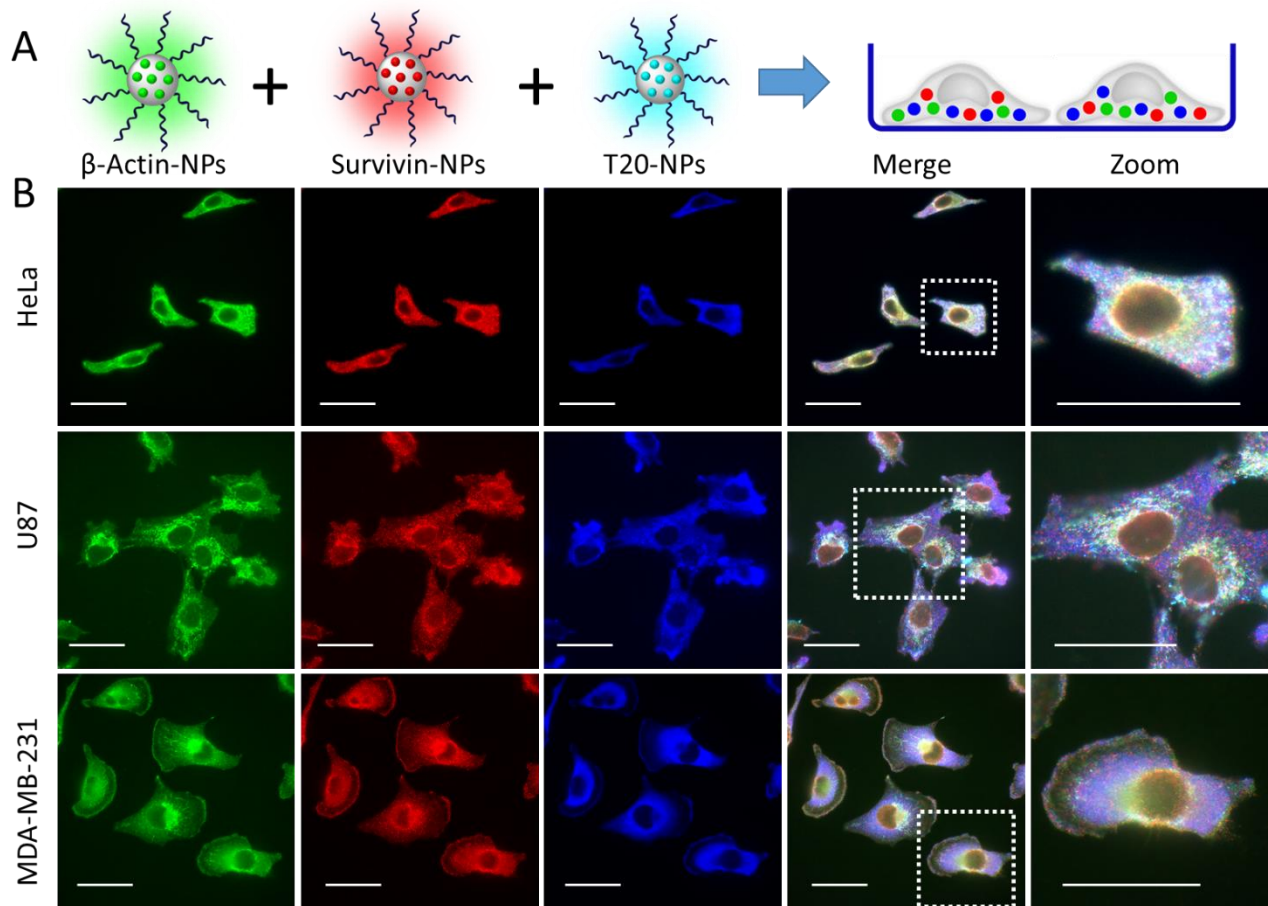


**Figure 8.** Multiplexed detection of mRNA sequences in fixed cells by AmpliFISH. (A) General principle and (B) Corresponding epi-fluorescence images of three nanoprobe (the same as in Figure 7)  $\beta$ -actin-NPs (green), survivin-NPs (red) and T20-NPs (blue) in three cell lines: HeLa (upper row), U87 (middle row) and MDA-MB-231 (lower row). Merge of three channels and corresponding zoomed images of cells are also shown (last two columns). A mixture of the 3 different NPs at 100 nM (total dye concentration) was added to cells during 1h, then washed 2 times before the observations. Scale bar: 50  $\mu$ m.

**Quantification and single-particle analysis.** We explored a possibility to quantify the observed fluorescence inside the HeLa cells with different DNA-NPs loaded with the same dye R18/F5. In addition to  $\beta$ -actin, survivin and A20, we prepared nanoprobe functionalized with another non-coding capture sequence (NP-NS) that does not correspond to any mRNA in HeLa cells. Using spinning-disk fluorescence microscopy, we recorded different planes of the cells and then summed all stacks together. The resulting images could clearly show the strong signal from  $\beta$ -actin-NPs, then

lower signal from survivin-NPs and practically no signal from non-coding sequence NS-NPs and A20-NPs (Figure 9A). Quantitative analysis confirmed these observations showing that the average signal decreased in the following order:  $\beta$ -actin-NP  $\gg$  survivin-NP  $\gg$  NS-NP  $>$  A20-NP (Figure 9B). RT-qPCR of the cells revealed that mRNA of  $\beta$ -actin was much more abundant (Ct = 15.2) than that of survivin (Ct = 24.8), supporting our FISH data. However, the differences revealed by RT-qPCR were significantly larger than those observed by the AmpliFISH method. Therefore, we consider that our approach at this step remains semi-quantitative. One should also note that, NS-NPs showed a bit higher signal than A20-NPs, which indicates that a part of the signal here could originate from off-target interactions of the non-coding sequence. Taking into account that the presence of competitive sequence can completely block the binding of corresponding DNA-NPs, we can conclude that non-specific binding of NPs could be related to some off-target hybridization with shorter nucleic acid sequences, which is a common problem of FISH technique.<sup>41,88</sup> This could explain why at the current state our method remains semi-quantitative.

The remaining question regarding our DNA-NPs in cells was whether the observed spots correspond to individual NPs. In the wide-field microscopy images (Figures 7 and 8), it was difficult to identify single particles because of poor Z-resolution and strong contribution of out of focus NPs to the final images. Therefore, we used spinning disk microscopy to record Z-stack of image planes of cells labelled with survivin-NPs and then reconstructed 3D images. In the 3D image (Figure 9C, Video S1) and the individual XY image plane (Figure 9D), one could clearly see individual dots distributed all around the cells, except nucleus, where NPs cannot really penetrate. In addition, we recorded videos from one focal plane of HeLa cells labelled with actin-NPs using spinning disk microscopy. We found that majority of bright dots (with acceptance of some larger spots) showed some signal fluctuation/blinking (Video S2). This fluorescence intermittence is typical for individual acrylate-based R18/F5 loaded NPs due to cooperative effects of dyes inside the polymeric particle.<sup>78</sup> Therefore, we can conclude that these dots correspond to single particles immobilized inside the cells through interactions with the target.

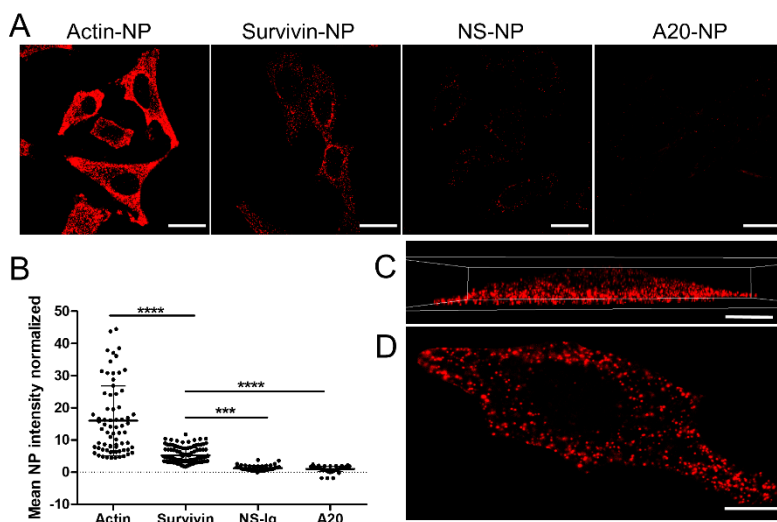


**Figure 9.** Imaging of HeLa cells using AmpliFISH with a spinning-disk microscopy and quantification of the signal from mRNA targets. (A) Z-projection of multiple images of HeLa cells stained with different DNA-NPs. Scale bar: 30  $\mu$ m. (B) Quantification of total fluorescence intensity from DNA-NPs for four different target mRNA sequences. At least 100 cells were analyzed per condition in 3 independent measurements. \*\*\* p < 0.001, \*\*\*\* p < 0.0001. (C) 3D reconstruction of

HeLa cells labelled with survivin-NPs. (D) Selected X-Y plane of the same cell as in (C) obtained by spinning-disk microscopy. Scale bar (C,D): 12  $\mu\text{m}$ .

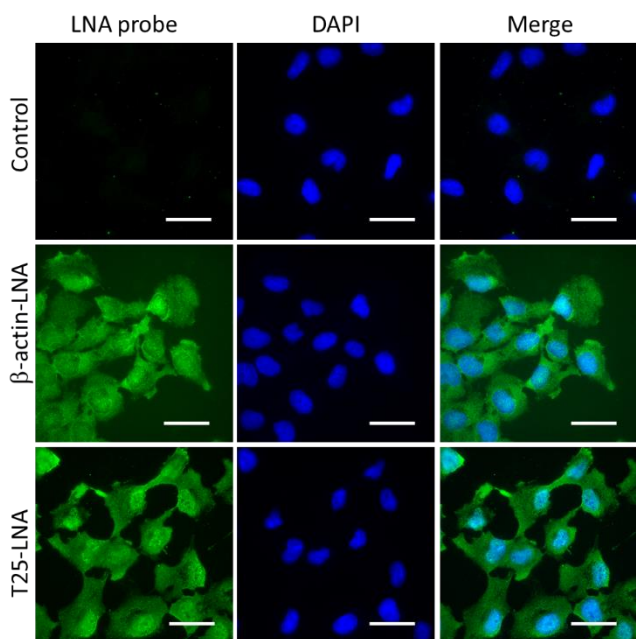


**Figure 10.** Commercial LNA probes at 25 nM for the detection of actin mRNA and poly (A) tails in U87 cells. Epifluorescence images of the FISH LNA probes and nuclei (DAPI) as well as the superposition (merge) of the 2 images (Scale: 50  $\mu\text{m}$ ).

**Comparison with a classical FISH method.** To benchmark the performance of AmpliFISH, a commercial FISH technique was used, employing locked nucleic acid (LNA) probes (Qiagen). The LNA technology provides improved discriminating capacity of FISH probes and thus improved sensitivity and specificity to the RNA targets.<sup>89</sup> Two types of LNA probes were tested: LNA T25 in order to target poly(A) of mRNA and LNA  $\beta$ -actin which groups together several sequences targeting actin mRNA. These two types of probes are coupled to digoxigenin (3' DIG) to allow indirect detection of mRNA targets (primary antibody then secondary antibody coupled to Alexa Fluor 488). The results obtained for these two probes as well as the negative control (absence of probe) for the U87 line are illustrated in Figure 10. On the one hand, there is indeed an absence of fluorescence signal for the negative control without LNA probes, ruling out non-specific interactions in the cells. On the other hand, a fluorescence signal is obtained for the LNA probes in the fixed and permeabilized U87MG cells, in the cytosol and in the nucleus. Unlike DNA-NPs, these probes are capable to detect their target in the nucleus, owing to their smaller size. However, the key difference was the obtained signal with the commercial probes was 8 times lower compared to that obtained with our green emission DNA-NPs loaded with Rh110-18/F12. Taking into account that our red NPs loaded with R18/F5 are 25 brighter than the green ones (see above), our AmpliFISH technique based on R18/F5 should provide 200-fold stronger signal compared to LNA FISH method. This drastic difference originates from the much higher brightness of our NPs (80-300 dyes per NP) compared to the fluorescently labelled antibodies. In addition, our technique is much simpler and faster compared to the commercial FISH comprised of >20 steps before microscopy accompanied by multiple washes between each step.

## Conclusions

Development of simple and direct methods for detection of mRNA inside the cells, which could accelerate biological and biomedical research and clinical diagnostics, remains a high challenge. To address this problem, we propose an amplified FISH methodology (AmpliFISH): ultrabright DNA-functionalized polymeric NPs are specially designed to penetrate cells and detect their intracellular mRNA targets. We synthesized NPs of different sizes and polymeric matrices. We found that the size of NPs below 20 nm is crucial for penetration and mRNA targeting in the fixed and permeabilized cells. Moreover, the nature of the polymer can drastically influence non-specific interactions, which allowed us to select polymeric NPs showing highest specificity. The obtained DNA-NPs enable sequence-specific detection and imaging of mRNA encoding  $\beta$ -actin, survivin as well as its poly(A) tail, based on a very simple protocol of cell preparation and short incubation with NPs. Moreover, combination of three different colors enables simultaneous detection of three mRNA targets within the same cell, showing feasibility of simple multiplexing single cell transcriptome analysis. Importantly, each cancer cell line displayed a characteristic intracellular distribution of the three mRNA sequences, like a cell fingerprint. Moreover, the method allows semi-quantitative analysis of mRNA in cells, although an additional dedicated study will be required to make it a truly quantitative single-cell mRNA detection method. Single-particle video microscopy confirmed that the majority of the intracellular signal corresponds to individual particles, which should enable mRNA detection with single-molecule sensitivity. Comparison with the commercial FISH technique based on LNA oligonucleotides showed that our method has multiple advantages: (i) it provides 8-200-fold stronger signal (dependent on the NP color); (ii) it is based on 3 steps *vs.* ~20 steps in the commercial technique as well as much shorter time. Thus, the developed AmpliFISH approach has the potential to significantly improve the current methods of transcriptomic analysis at the single cell level, which is important for both biological research and clinical diagnostics.

## Materials and methods

**Chemical synthesis.** Chemicals were purchased from either Sigma Aldrich, Alfa Aesar or Thermofisher Scientific. NMR spectra were recorded at 20°C on Bruker Avance III 400MHz spectrometer and chemical shifts were reported as delta scale in ppm relative to  $\text{CHCl}_3$  ( $\delta = 7.26$  ppm) for  $^1\text{H}$  NMR and  $\text{CDCl}_3$  ( $\delta = 77.16$  ppm) for  $^{13}\text{C}$  NMR. Mass spectra were obtained using an Agilent Q-TOF 6520 mass spectrometer. Polymers PMMA-AspN3-1.6%, PMMA-AspN3-5% and PEMA-AspN3 were synthesized as described previously<sup>51,52</sup> Rhodamine B octadecyl ester trakis(pentafluorophenyl)borate (R18/F5) and DiD/F12 were synthesized by ion exchange and purified by column chromatography as described previously.<sup>77,81</sup> Rhodamine 110 octadecyl ester (Rh110-C18/Cl) was synthesized by coupling of Rhodamine 110 chloride and 1-octadecanol in the presence of sulfuric acid, followed by column chromatography purification as described elsewhere.<sup>90</sup> Rhodamine 110 octadecyl ester tetrakis[3,5-bis(1,1,1,3,3,3-hexafluoro-2-methoxy-2-propyl)phenyl]borate trihydrate (Rh110-C18/F12) was obtained by the ion exchange of obtained Rh110-C18/Cl with a sodium tetrakis[3,5-bis(1,1,1,3,3,3-hexafluoro-2-methoxy-2-propyl)phenyl]borate trihydrate (F12) followed by purification on preparative TLC using dichloromethane/methanol 95/5 as eluent.

**Preparation of NPs.** Sodium phosphate monobasic (>99.0%, Sigma-Aldrich) and sodium phosphate dibasic dihydrate (>99.0%, Sigma- Aldrich) were used to prepare 20 mM phosphate buffers. Sodium

tetraborate decahydrate (>99.0%, Sigma- Aldrich) was used to prepare borate buffer. Final pH was adjusted with 0.1 M hydrochloride acid or 0.1 M sodium hydroxide. Milli-Q water (Millipore) was used in all experiments.

**NP-PMMA-MA-1.6%.** 100  $\mu\text{L}$  of the polymer solution in acetonitrile (2 mg  $\text{mL}^{-1}$  with 30 wt% of R18/F5 relative to the polymer) were added quickly using a micropipette to 900  $\mu\text{L}$  of phosphate buffer 20mM, pH 7.4 under shaking (Thermomixer comfort, Eppendorf, 1100 rpm). Then, the residues of acetonitrile were evaporated.

**NP-PMMA-MA-5% and NP-PEMA-MA (multicolor).** 50  $\mu\text{L}$  of the polymer solution in acetonitrile (2 mg  $\text{mL}^{-1}$  containing Rh110-C18/F12 at 30 wt%, R18/F5 at 50 wt% or DiD/F12 at 30 wt% relative to the polymer) were added quickly using a micropipette to 450  $\mu\text{L}$  of 10 mM borate buffer, pH 9 at 21 °C under shaking (Thermomixer comfort, Eppendorf, 1100 rpm). While continuing mixing, 500  $\mu\text{L}$  of 20 mM phosphate buffer, pH 6 were added. Then, the residues of acetonitrile were evaporated. The particle solution was then diluted 2-fold with the 20 mM of phosphate buffer, pH 7.4.

**General protocol for functionalization of NPs with DNA.** Lyophilized single strand DNA sequences were purchased from IBA GmbH, dissolved in Milli-Q water, aliquoted and stored at -20 °C for further experiments. Aliquots of corresponding DNA-DBCO (concentration of 60  $\mu\text{M}$  in the reaction mixture) were added to 200  $\mu\text{L}$  of corresponding nanoparticles. The reaction was mixed and kept overnight at 40 °C without shaking protected from light. Then the reaction was cooled down to room temperature. In case of NPs with double strand, to 100 $\mu\text{L}$  of the reaction the aliquot of DNA-target sequence in ratio 1:1 with DNA-DBCO was added and the mixture was heated to 70 °C in a water bath for 3 min. To complete hybridization the reaction was cooled down to room temperature and kept in the dark for 2 h. Then, in case of single-strand nanoparticles the mixture was diluted with 20 mM phosphate buffer to 4 mL. In case of the double strand nanoparticles, the mixture was diluted with 20 mM phosphate buffer containing 12 mM  $\text{MgCl}_2$  and 30 mM NaCl to 4 mL. Both types of NPs were purified by centrifugation using centrifuge filters (Amicon, 0.5 mL, 100 kD, Sigma-Aldrich) on 1000 g at 20 °C for 2 min. The procedure of centrifugation was repeated 5 times to remove the non-reacted oligonucleotides using corresponding buffer. The obtained functionalized DNA-NPs were kept in the dark at 4 °C.

The oligonucleotide sequences used in this study are shown below:

SurC-DBCO, 5'- CCC AGC CTT CCA GCT CCT TGA - (DBCO) - 3'.

SurC-Target, 5'- CAA GGA GCT GGA AGG CTG GG - 3'.

SurC-Competitive, 5'- CCC AGC CTT CCA GCT CCT TGA - 3'.

Actin-DBCO, 5' - CTG ACC CAT GCC CAC CAT CA - (DBCO) - 3'.

Actin-Target, 5' - TGA TGG TGG GCA TGG GTC AG - 3'.

Actin-Competitive, 5' - CTG ACC CAT GCC CAC CAT CA - 3'.

T20-DBCO, 5'- TT TTT TTT TTT TTT TTT TT-(DBCO) - 3'.

T20, 5'- TT TTT TTT TTT TTT TTT TT - 3'.

A20-DBCO, 5'- AAA AAA AAA AAA AAA AAA AA-(DBCO) - 3'.

**Characterization of NPs.** Dynamic light scattering (DLS) measurements were performed on a Zetasizer Nano ZSP (Malvern Instruments S.A.). The Zetasizer software provided with standard cumulates and size distribution by volume analysis was used to characterize nanoparticles by DLS. For the data analysis, the following parameters were used: for the solvent (water) – temperature 25

°C, refractive index RI 1.33, and viscosity 0.8872 cP. Nanoparticles were assumed to be all homogenous and spherical in shape. Absorption spectra were recorded on a Cary 5000 scan UV-visible spectrophotometer (Varian). Excitation, emission spectra and anisotropy were recorded on a FS5 Spectrofluorometer (Edinburg Instruments). For standard recording of fluorescence spectra, the excitation wavelength was set to 470 nm (Rh110-C18/F12), 530 nm (R18/F5) and 640 nm (DiD/F12). The fluorescence spectra were corrected for detector response and lamp fluctuations. Quantum yields of NPs and QDots were calculated using fluorescein in 10 mM NaOH (QY = 1.0), Rhodamine 101 in methanol (QY = 1.0)<sup>91</sup> and DiD in methanol (QY = 0.33)<sup>92</sup> as the corresponding references.

**Transmission electron microscopy (TEM).** Carbon-coated copper-rhodium electron microscopy grids with a 300 mesh (Euromedex, France) were surface treated with a glow discharge in amylamine atmosphere (0.45 mbar, 5 – 5.3 mA, 25 s) in an Elmo glow discharge system (Cordouan Technologies, France). Then, 5  $\mu$ L of the solution of NPs were deposited onto the grids and left for 2 min. The grids were then treated for 1 min with a 2% uranyl acetate solution for staining. They were observed with the Tecnai F20 electron microscope, equipped with a FEG operated at 200 keV. Areas covered with nanoparticles of interest were recorded at 29000x magnifications on a GATAN CCD 2K\*2K "US10001" camera. Image analysis was performed using the Fiji software.

**Single-particle fluorescence microscopy.** Immobilization of DNA-NPs and QDots was done as follows. The LabTek chamber (Borosilicate cover glass, eight wells, ThermoFisher Scientific) was washed 3 times with PBS followed by incubation with 200  $\mu$ L of BSA-Biotin (Sigma-Aldrich) 0.5 mg mL<sup>-1</sup> in PBS for 5 min. Then, BSA-biotin solution was removed, and the chamber was washed 3 times with 500  $\mu$ L of PBS. In case of nanoparticles immobilization, the chamber was incubated with 200  $\mu$ L of neutravidin (ThermoFisher Scientific) solution (0.5 mg mL<sup>-1</sup> in PBS) for 5 min and washed 3 times with 500  $\mu$ L of PBS. Then the chamber was incubated with 200  $\mu$ L of 1  $\mu$ M solution of A20-biotin in PBS for 5 min and washed 1 time with PBS and 2 times with 20 mM phosphate buffer. Then nanoprobe solution was deposited with proper concentration to achieve desired density and incubated for 1 hour at room temperature in the dark. Before measurements the chamber was washed 2 times with 20 mM phosphate buffer and covered with 200  $\mu$ L of the same buffer. In case of QDots immobilization, QDot525 Streptavidin Conjugate, QDot605 Streptavidin Conjugate and QDot705 Streptavidin Conjugate (ThermoFisher Scientific) were diluted to 10 pM final concentration in PBS and 300  $\mu$ L was added to the chamber. After 1 h of incubation, the chamber was washed 3 times with 500  $\mu$ L and filled with 200  $\mu$ L of PBS.

Single-particle microscopy measurements were performed in the epi-fluorescence mode using Nikon Ti-E inverted microscope with a 100x objective (Apo TIRF, oil, NA 1.49, Nikon). The excitation was provided by light emitting diodes (SpectraX, Lumencor) with the following wavelength and power density: 470 nm at 14 and 23 W cm<sup>-2</sup> for Rh110-C18/F12 NPs and QDot525, respectively; 550 nm at 0.24 and 24 W cm<sup>-2</sup> for R18/F5 NPs and QDot605, respectively and 640 nm at 1.1 and 17 W cm<sup>-2</sup> for DiD/F12 NPs and QDot705. The emission filters used were the following: The exposure time was set to 400 ms per image frame. The fluorescence signal was recorded with a Hamamatsu Orca Flash 4 camera. Corresponding power densities and light emitting diodes used for each nanoparticle and QDot samples are presented in the table below.

Single-particle analysis was performed using the Fiji software. Particle locations were detected through a Fiji routine applied to a projection (maximum intensity) of all obtained frames per experiment. After the automatic background subtraction, the mean intensities of circular regions of interest with a diameter of 8 pixels around the found particle locations were then measured. At least

three image sequences (245 pixel  $\times$  245 pixel) per condition with, on average, 1000-2000 particles per sample were analyzed.

**Cell culture.** HeLa cells (ATCC CCL-2) were grown in Dulbecco's modified Eagle's medium low glucose (DMEM, Gibco), supplemented with 10% fetal bovine serum (FBS, Dutscher), 1% L-glutamine (Lonza) and 1% penicillin-streptomycin (Lonza). The human glioblastoma cell line U87 (ATCC) was maintained in Minimum Essential Medium (MEM, Gibco) supplemented with 10% fetal bovine serum, 1% L-glutamine, 1% sodium pyruvate (Lonza) and 1% non-essential amino-acid (Lonza). The human breast cancer cell line MDA-MB-231 (ATCC) was grown in Minimum Essential Medium (MEM, Gibco) supplemented with 10% fetal bovine serum and 1% of ultraglutamine (Lonza). All cell lines were maintained at 37°C in a humidified atmosphere containing 5% CO<sub>2</sub>. For the different experiments, cells were seeded in 8 well LabTek (ThermoFisher) at 8 000 cells/well overnight.

**Cell fixation and permeabilization.** For the fixation step, a standard protocol of immunofluorescence was applied. First, cells were washed one time with DPBS (Lonza) and incubated with 4 % PFA during 12 min at 37°C. Cells were then washed 2 times with DPBS and incubated 1 min at RT with 0.1% Triton x100. Then, cells were washed 2 times with DPBS and incubated in 3% BSA/DPBS (Sigma) for 1h30 at RT. The final step was to remove the 3% BSA/DPBS solution and incubated cells in DPBS. The fixed cells can be used just after fixation or can be kept at 4°C until their utilization.

**In situ hybridization with DNA-NPs.** Independently of the DNA sequence used, DNA-NPs were first diluted to 100 nM concentration in 0.1% BSA/DPBS. Then, DPBS from the fixed permeabilized cells was removed and the diluted DNA-NPs were added to the cells for 1h at RT or 37 °C. Then, cells were washed 2 times with 0.1% BSA/DPBS to remove the DNA-NPs that were not hybridized with the RNA target and then cells were observed by the microscope in 0.1% BSA/DPBS.

In case of competition experiments, cells were pre-incubated for 1 hour at RT with a complementary DNA sequence to actin or survivin mRNA target at 100 nM diluted in 0.1% BSA/DPBS. Without any washed step, NPs were directly added on cells, followed by the above described protocol.

**Cell imaging.** At the beginning of the study, cells and NPs were observed with TIRF mode using a Nikon Ti-E inverted microscope with a 100 $\times$  objective (Apo TIRF, oil, NA 1.49, Nikon). Excitation wavelength was 550 nm with a power density of 26 W cm<sup>-2</sup>; emission was recorded with 600/50 nm band-pass filter. Then, images were acquired in epi-fluorescence mode with a Nikon Ti-E inverted microscope, with a 60x oil objective (NA 1.4, Nikon) and a Hamamatsu Orca Flash 4 sCMOS camera. The excitation was provided by light emitting diodes (LED, SpectraX, Lumencor). Acquisition settings were: for Rh110-C18/F12 NPs (ex. 470 nm; emission: 531/40 nm band-pass filter) with an excitation power density of 5 W cm<sup>-2</sup> and exposure time of 300 ms, for R18/F5 NPs (ex. 550 nm; emission: 600/50 nm band-pass filter) with an excitation power density of 3 W cm<sup>-2</sup> and exposure time of 200 ms and for DiD/F12 NPs (ex. 638 nm; emission: 705/72 nm band-pass filter) with an excitation power density of 1.3 W cm<sup>-2</sup> and exposure time of 200 ms. The images were recorded using NIS Elements and then processed with ImageJ software. Co-localization analysis was performed using Manders' coefficient with JACoP plugin in Fiji software. A threshold was applied for each channel of all images (1685 to Actin, 1613 to Survivin and 1531 to T20).

Quantitative cellular imaging with R18/F5 NPs (Figure 9) was performed using a Nikon Ti-E inverted microscope, equipped with CFI Plan Apo  $\times 60$  oil (NA = 1.4) objective, X-Light spinning disk module (CREST Optics), and a Hamamatsu Orca Flash 4 sCMOS camera with 600/50 nm band-pass filter. The excitation in confocal mode was provided by a 532 nm diode laser (OXXIUS). The exposure time in confocal mode was set to 500 ms per image frame. All the images were recorded using NIS Elements and then processed using Fiji software. Background was removed in all images using a filter rolling ball with 20 pixels' radius and a sliding paraboloid shape. All images are presented with the same brightness and contrast. Mean fluorescence intensity was measured on the 3D stack for around 100 cells per conditions from 3 independent experiments. Statistical analysis was done with ANOVA algorithm.

**RT-qPCR.** Cell line selection was based on surviving mRNA expression. Two days before RNA extraction,  $10^6$  cells were seeded in 100 mm Petri dishes. Total RNA was isolated using a miRNeasy Mini Kit (Qiagen) following the protocol provided by the manufacturer. The final volume of elution was 40  $\mu$ L. The quantity of total RNA was performed using a Nanodrop (Thermo Scientific). RNA samples were aliquoted and stored at  $-80^\circ\text{C}$ . Then, 1  $\mu$ g of RNA extracted was transcribed into cDNA using miScript II Reverse Transcription Kit (Qiagen). mRNA expression was evaluated by relative quantitative RT-qPCR analysis using the Fast SYBR Green Master Mix PCR kit (Qiagen) and the StepOne Plus Real time PCR system (Applied Biosystem), according to the manufacturer protocol. The primers used were:  $\beta$ -actin (RT<sup>2</sup>qPCR Primer Assay for Human ACTB, NM\_001101, Qiagen) and BIRC5 (RT<sup>2</sup>qPCR Primer Assay for Human NM\_001168, Qiagen). RT-PCR was carried out with Human RNA 18S (5'-TGTGGTGTGAGGAAAGCAG-3' and 5'-TCCAG ACCATTGGCTAGGAC-3') Invitrogen) as internal reference. Target cDNA expression was quantified using the comparative  $\Delta\Delta\text{Ct}$  method with 18S rRNA as an internal control.

**FISH with commercial LNA probe.** To compare our results with commercial *in situ* hybridization, poly(T)<sub>25</sub> and  $\beta$ -actin LNA probes (Qiagen) were used coupled with DIG as described in the manufacturer protocol (Exiqon). The DIG proteins were detected thanks to indirect method, in order to amplify the signal with anti-DIG primary antibody and secondary antibody coupled with fluorochromes. Briefly, the first day, U87MG were seeded on 22 mm diameter coverslips deposited on 6 well plates and let rest overnight. Then, cells were washed once with DPBS and fixed with 4 % PFA (Thermo Scientific) / 5% acetic acid (Sigma) in DPBS for 15 min. U87 cells were washed 2x5 min in DPBS, treat with pepsin (Merck) (0.1% in 10 mM HCl) for 1 min at  $37^\circ\text{C}$  and washed again 2 times with water. At this step, cells were dehydrated through 70 %, 90 % and 100 % ethanol et let them dry few seconds. Then, 25  $\mu$ L probes diluted at 25 nM in hybridization buffer (50% deionized formamide (Merck), 2x SSC (ThermoFisher), 50 mM sodium phosphate (Merck), 10 % Dextran sulfate (Merck) were put on a slide and covered with the coverslips. The montage was heated at  $80^\circ\text{C}$  for 75 secs and the hybridization step was performed for 30 min in a humid chamber at  $55^\circ\text{C}$  for poly(T)<sub>25</sub> probes and at  $62^\circ\text{C}$  for  $\beta$ -actin probes. Then, coverslips were washed with 2xSSC contained 0.1% Tween 20 and washed 3x 5 min with 0.1x SSC at  $65^\circ\text{C}$ . Cells were dehydrated through 70 %, 90 % and 100 % ethanol et let them dry few seconds. Finally, U87MG cells were incubated with 3% BSA/DPBS (Sigma) for 1h30 at RT, followed by the anti-DIG from Mouse IgG primary antibody (Sigma) at 1 $\mu$ g/mL in 3 % BSA/DPBS overnight at  $4^\circ\text{C}$  in a humid chamber. The day after, cells were washed 3x5 min in DPBS and incubated with Goat anti-mouse IgG secondary antibody coupled with Alexa Fluor 488 nm (ThermoFisher) diluted at 1  $\mu$ g/mL and DAPI (ThermoFisher) diluted at 5  $\mu$ g/mL for 45 min. After 3 x 5 min of washing with DPBS, cells were

mounted on a microscope slide with Mounting Medium (Dako) and let dry in the dark overnight. Finally, coverslips were observed with epi-fluorescence mode with a Nikon Ti-E inverted microscope, with a  $\times 60$  oil objective (numerical aperture = 1.4) and a Hamamatsu Orca Flash 4 sCMOS camera. The settings were: DAPI (excitation 395 nm; emission 468-552 nm) with a power of 30 % and exposure time of 200 ms and Alexa 488 nm (excitation 470 nm; emission 491-571 nm) with a power of 90 % and exposure time of 200 ms. The images were recorded using NIS Elements and then processed with ImageJ software.

## ASSOCIATED CONTENT

### Supporting Information

The Supporting Information is available free of charge at <https://pubs.acs.org/doi/>.

Additional characterization data, cellular images and colocalization analysis.

### Declaration of competing interests

Nina Melnychuk, Andreas Reisch and Andrey S. Klymchenko are inventors on a patent application related to this technology (European patent application no. 18305253.9). The remaining authors declare no competing interests.

### Acknowledgements

This work was supported by the European Research Council ERC Consolidator grant BrightSens 648525, ERC Proof of concept grand AmpliFISH 899928 and SATT Conectus maturation grant NanoAntenna. We thank Corinne Crucifix from the FRISBI platform for her help with the electron microscopy and Anne Runser for help with polymer synthesis.

### References

1. Michelini, F.; Jaliha, A. P.; Francia, S.; Meers, C.; Neeb, Z. T.; Rossiello, F.; Gioia, U.; Aguado, J.; Jones-Weinert, C.; Luke, B.; Biamonti, G.; Nowacki, M.; Storici, F.; Carninci, P.; Walter, N. G.; di Fagagna, F. D. From "Cellular" RNA to "Smart" RNA: Multiple Roles of RNA in Genome Stability and Beyond. *Chem. Rev.* **2018**, *118*, 4365-4403.
2. Fatica, A.; Bozzoni, I. Long Non-Coding RNAs: New Players in Cell Differentiation and Development. *Nat. Rev. Genet.* **2014**, *15*, 7-21.
3. Xia, Y. Q.; Zhang, R. L.; Wang, Z. L.; Tian, J.; Chen, X. Y. Recent Advances in High-Performance Fluorescent and Bioluminescent RNA Imaging Probes. *Chem. Soc. Rev.* **2017**, *46*, 2824-2843.
4. Dean, K. M.; Palmer, A. E. Advances in Fluorescence Labeling Strategies for Dynamic Cellular Imaging. *Nat. Chem. Biol.* **2014**, *10*, 512-523.
5. Tyagi, S. Imaging Intracellular RNA Distribution and Dynamics in Living Cells. *Nat. Methods* **2009**, *6*, 331-338.
6. Femino, A. M.; Fay, F. S.; Fogarty, K.; Singer, R. H. Visualization of Single RNA Transcripts *in Situ*. *Science* **1998**, *280*, 585-590.
7. Saliba, A.-E.; Westermann, A. J.; Gorski, S. A.; Vogel, J. Single-Cell RNA-Seq: Advances and Future Challenges. *Nucleic Acids Res.* **2014**, *42*, 8845-8860.

8. Haque, A.; Engel, J.; Teichmann, S. A.; Lonnberg, T. A Practical Guide to Single-Cell RNA-Sequencing for Biomedical Research and Clinical Applications. *Genome Med.* **2017**, *9*, 75.
9. Bertrand, E.; Chartrand, P.; Schaefer, M.; Shenoy, S. M.; Singer, R. H.; Long, R. M. Localization of Ash1 mRNA Particles in Living Yeast. *Mol. Cell* **1998**, *2*, 437-445.
10. Paige, J. S.; Wu, K. Y.; Jaffrey, S. R. RNA Mimics of Green Fluorescent Protein. *Science* **2011**, *333*, 642-646.
11. Neubacher, S.; Hennig, S. RNA Structure and Cellular Applications of Fluorescent Light-Up Aptamers. *Angew. Chem. Int. Ed.* **2019**, *58*, 1266-1279.
12. Filonov, G. S.; Moon, J. D.; Svensen, N.; Jaffrey, S. R. Broccoli: Rapid Selection of an RNA Mimic of Green Fluorescent Protein by Fluorescence-Based Selection and Directed Evolution. *J. Am. Chem. Soc.* **2014**, *136*, 16299-16308.
13. Bouhedda, F.; Fam, K. T.; Collot, M.; Autour, A.; Marzi, S.; Klymchenko, A.; Ryckelynck, M. A Dimerization-Based Fluorogenic Dye-Aptamer Module for RNA Imaging in Live Cells. *Nat. Chem. Biol.* **2020**, *16*, 69-76.
14. Sunbul, M.; Lackner, J.; Martin, A.; Englert, D.; Hacene, B.; Grun, F.; Nienhaus, K.; Nienhaus, G. U.; Jaschke, A. Super-Resolution RNA Imaging Using a Rhodamine-Binding Aptamer with Fast Exchange Kinetics. *Nat. Biotechnol.* **2021**, *39*, 686-690.
15. Gall, J. G.; Pardue, M. L. Formation and Detection of RNA-DNA Hybrid Molecules in Cytological Preparations. *Proc. Natl. Acad. Sci. U. S. A.* **1969**, *63*, 378-383.
16. John, H. A.; Birnstiel, M. L.; Jones, K. W. RNA-DNA Hybrids at the Cytological Level. *Nature* **1969**, *223*, 582-587.
17. Bauman, J. G.; Wiegant, J.; Borst, P.; van Duijn, P. A New Method for Fluorescence Microscopical Localization of Specific DNA Sequences by *in Situ* Hybridization of Fluorochromelabelled RNA. *Exp. Cell Res.* **1980**, *128*, 485-490.
18. Langer-Safer, P. R.; Levine, M.; Ward, D. C. Immunological Method for Mapping Genes on Drosophila Polytene Chromosomes. *Proc. Natl. Acad. Sci. U. S. A.* **1982**, *79*, 4381-4385.
19. Cui, C.; Shu, W.; Li, P. Fluorescence *in Situ* Hybridization: Cell-Based Genetic Diagnostic and Research Applications. *Front. Cell Dev. Biol.* **2016**, *4*, 89.
20. Urbanek, M. O.; Krzyzosiak, W. J. RNA FISH for Detecting Expanded Repeats in Human Diseases. *Methods* **2016**, *98*, 115-123.
21. Raj, A.; Rinn, J. L. Illuminating Genomic Dark Matter with RNA Imaging. *Cold Spring Harb. Perspect. Biol.* **2019**, *11*, a032094.
22. Cui, C.; Shu, W.; Li, P. Fluorescence *in Situ* Hybridization: Cell-Based Genetic Diagnostic and Research Applications. *Front. Cell Dev. Biol.* **2016**, *4*, 89.
23. Shaffer, S. M.; Joshi, R. P.; Chambers, B. S.; Sterken, D.; Biaesch, A. G.; Gabrieli, D. J.; Li, Y.; Feemster, K. A.; Hensley, S. E.; Issadore, D.; Raj, A. Multiplexed Detection of Viral Infections Using Rapid *in Situ* RNA Analysis on a Chip. *Lab Chip* **2015**, *15*, 3170-3182.
24. Kwon, S. Single-Molecule Fluorescence *in Situ* Hybridization: Quantitative Imaging of Single RNA Molecules. *BMB Rep.* **2013**, *46*, 65-72.
25. Shaffer, S. M.; Wu, M.-T.; Levesque, M. J.; Raj, A. Turbo FISH: A Method for Rapid Single Molecule RNA FISH. *PLOS ONE* **2013**, *8*, e75120.
26. Femino, A.; Fay, F. S.; Fogarty, K.; Singer, R. H. Visualization of Single RNA Transcripts *in Situ*. *Science* **1998**, *280*, 585-590.
27. Raj, A.; van den Bogaard, P.; Rifkin, S. A.; van Oudenaarden, A.; Tyagi, S. Imaging Individual mRNA Molecules Using Multiple Singly Labeled Probes. *Nat. Methods* **2008**, *5*, 877-879.
28. Jensen, E. Technical Review: *In Situ* Hybridization. *Anat. Rec.* **2014**, *297*, 1349-1353.
29. Sinnamon, J. R.; Czaplinski, K. RNA Detection *in Situ* with FISH-Stics. *RNA* **2014**, *20*, 260-266.
30. Xia, C.; Babcock, H. P.; Moffitt, J. R.; Zhuang, X. Multiplexed Detection of RNA Using MerFISH and Branched DNA Amplification. *Sci. Rep.* **2019**, *9*, 7721.
31. Wang, F.; Flanagan, J.; Su, N.; Wang, L. C.; Bui, S.; Nielson, A.; Wu, X.; Vo, H. T.; Ma, X. J.; Luo, Y. RNAscope: A Novel *in Situ* RNA Analysis Platform for Formalin-Fixed, Paraffin-Embedded Tissues. *J. Mol. Diagn.* **2012**, *14*, 22-29.

32. Qing, Z. H.; Xu, J. Y.; Hu, J. L.; Zheng, J.; He, L.; Zou, Z.; Yang, S.; Tan, W. H.; Yang, R. H. *In Situ* Amplification-Based Imaging of RNA in Living Cells. *Angew. Chem. Int. Ed.* **2019**, *58*, 11574-11585.
33. Lizardi, P. M.; Huang, X.; Zhu, Z.; Bray-Ward, P.; Thomas, D. C.; Ward, D. C. Mutation Detection and Single-Molecule Counting Using Isothermal Rolling-Circle Amplification. *Nat. Genet.* **1998**, *19*, 225-232.
34. Choi, H. M. T.; Chang, J. Y.; Trinh, L. A.; Padilla, J. E.; Fraser, S. E.; Pierce, N. A. Programmable *in Situ* Amplification for Multiplexed Imaging of mRNA Expression. *Nat. Biotechnol.* **2010**, *28*, 1208-1212.
35. Choi, H. M. T.; Beck, V. A.; Pierce, N. A. Next-Generation *in Situ* Hybridization Chain Reaction: Higher Gain, Lower Cost, Greater Durability. *ACS Nano* **2014**, *8*, 4284-4294.
36. Kishi, J. Y.; Lapan, S. W.; Beliveau, B. J.; West, E. R.; Zhu, A.; Sasaki, H. M.; Saka, S. K.; Wang, Y.; Cepko, C. L.; Yin, P. Saber Amplifies FISH: Enhanced Multiplexed Imaging of RNA and DNA in Cells and Tissues. *Nat. Methods* **2019**, *16*, 533-544.
37. Kishi, J. Y.; Schaus, T. E.; Gopalkrishnan, N.; Xuan, F.; Yin, P. Programmable Autonomous Synthesis of Single-Stranded DNA. *Nat. Chem.* **2018**, *10*, 155-164.
38. Rouhanifard, S. H.; Mellis, I. A.; Dunagin, M.; Bayatpour, S.; Jiang, C. L.; Dardani, I.; Symmons, O.; Emert, B.; Torre, E.; Cote, A.; Sullivan, A.; Stamatoyannopoulos, J. A.; Raj, A. ClampFISH Detects Individual Nucleic Acid Molecules Using Click Chemistry-Based Amplification. *Nat. Biotechnol.* **2019**, *37*, 84-89.
39. Orjalo, A.; Johansson, H. E.; Ruth, J. L. Stellaris™ Fluorescence *in Situ* Hybridization (FISH) Probes: A Powerful Tool for mRNA Detection. *Nat. Methods* **2011**, *8*, i-ii.
40. Narrandes, S.; Xu, W. Gene Expression Detection Assay for Cancer Clinical Use. *J. Cancer* **2018**, *9*, 2249-2265.
41. Huber, D.; Voith von Voithenberg, L.; Kaigala, G. V. Fluorescence *in Situ* Hybridization (FISH): History, Limitations and What to Expect from Micro-Scale FISH? *Micro Nano Eng.* **2018**, *1*, 15-24.
42. Chinen, A. B.; Guan, C. M.; Ferrer, J. R.; Barnaby, S. N.; Merkel, T. J.; Mirkin, C. A. Nanoparticle Probes for the Detection of Cancer Biomarkers, Cells, and Tissues by Fluorescence. *Chem. Rev.* **2015**, *115*, 10530-10574.
43. Wolfbeis, O. S. An Overview of Nanoparticles Commonly Used in Fluorescent Bioimaging. *Chem. Soc. Rev.* **2015**, *44*, 4743-4768.
44. Howes, P. D.; Chandrawati, R.; Stevens, M. M. Colloidal Nanoparticles as Advanced Biological Sensors. *Science* **2014**, *346*, 1247390.
45. Reisch, A.; Klymchenko, A. S. Fluorescent Polymer Nanoparticles Based on Dyes: Seeking Brighter Tools for Bioimaging. *Small* **2016**, *12*, 1968-1992.
46. Algar, W. R.; Massey, M.; Rees, K.; Higgins, R.; Krause, K. D.; Darwish, G. H.; Peveler, W. J.; Xiao, Z.; Tsai, H.-Y.; Gupta, R.; Lix, K.; Tran, M. V.; Kim, H. Photoluminescent Nanoparticles for Chemical and Biological Analysis and Imaging. *Chem. Rev.* **2021**, *121*, 9243-9358.
47. Luan, J.; Seth, A.; Gupta, R.; Wang, Z.; Rathi, P.; Cao, S.; Gholami Derami, H.; Tang, R.; Xu, B.; Achilefu, S.; Morrissey, J. J.; Singamaneni, S. Ultrabright Fluorescent Nanoscale Labels for the Femtomolar Detection of Analytes with Standard Bioassays. *Nat. Biomed. Eng.* **2020**, *4*, 518-530.
48. Zhao, X. J.; Tapecc-Dytioco, R.; Tan, W. H. Ultrasensitive DNA Detection Using Highly Fluorescent Bioconjugated Nanoparticles. *J. Am. Chem. Soc.* **2003**, *125*, 11474-11475.
49. Hildebrandt, N.; Spillmann, C. M.; Algar, W. R.; Pons, T.; Stewart, M. H.; Oh, E.; Susumu, K.; Diaz, S. A.; Delehanty, J. B.; Medintz, I. L. Energy Transfer with Semiconductor Quantum Dot Bioconjugates: A Versatile Platform for Biosensing, Energy Harvesting, and Other Developing Applications. *Chem. Rev.* **2017**, *117*, 536-711.
50. Wu, W. B.; Bazan, G. C.; Liu, B. Conjugated-Polymer-Amplified Sensing, Imaging, and Therapy. *Chem* **2017**, *2*, 760-790.
51. Melnychuk, N.; Egloff, S.; Runser, A.; Reisch, A.; Klymchenko, A. S. Light-Harvesting Nanoparticle Probes for FRET-Based Detection of Oligonucleotides with Single-Molecule Sensitivity. *Angew. Chem. Int. Ed.* **2020**, *59*, 6811-6818.

52. Melnychuk, N.; Klymchenko, A. S. DNA-Functionalized Dye-Loaded Polymeric Nanoparticles: Ultrabright FRET Platform for Amplified Detection of Nucleic Acids. *J. Am. Chem. Soc.* **2018**, *140*, 10856-10865.
53. Ochmann, S. E.; Vietz, C.; Trofymchuk, K.; Acuna, G. P.; Lalkens, B.; Tinnefeld, P. Optical Nanoantenna for Single Molecule-Based Detection of Zika Virus Nucleic Acids without Molecular Multiplication. *Anal. Chem.* **2017**, *89*, 13000-13007.
54. Acuna, G. P.; Möller, F. M.; Holzmeister, P.; Beater, S.; Lalkens, B.; Tinnefeld, P. Fluorescence Enhancement at Docking Sites of DNA-Directed Self-Assembled Nanoantennas. *Science* **2012**, *338*, 506-510.
55. Vafaei, S.; Allabush, F.; Tabaei, S. R.; Male, L.; Dafforn, T. R.; Tucker, J. H. R.; Mendes, P. M. Förster Resonance Energy Transfer Nanoplatform Based on Recognition-Induced Fusion/Fission of DNA Mixed Micelles for Nucleic Acid Sensing. *ACS Nano* **2021**, *15*, 8517-8524.
56. He, D.; Wong, K.-W.; Dong, Z.; Li, H.-W. Recent Progress in Live Cell mRNA/MicroRNA Imaging Probes Based on Smart and Versatile Nanomaterials. *J. Mater. Chem. B* **2018**, *6*, 7773-7793.
57. Prigodich, A. E.; Seferos, D. S.; Massich, M. D.; Giljohann, D. A.; Lane, B. C.; Mirkin, C. A. Nano-Flares for mRNA Regulation and Detection. *ACS Nano* **2009**, *3*, 2147-2152.
58. Seferos, D. S.; Giljohann, D. A.; Hill, H. D.; Prigodich, A. E.; Mirkin, C. A. Nano-Flares: Probes for Transfection and mRNA Detection in Living Cells. *J. Am. Chem. Soc.* **2007**, *129*, 15477- 15479.
59. Briley, W. E.; Bondy, M. H.; Randeria, P. S.; Dupper, T. J.; Mirkin, C. A. Quantification and Real-Time Tracking of RNA in Live Cells Using Sticky-Flares. *Proc. Natl. Acad. Sci. U. S. A.* **2015**, *112*, 9591-9595.
60. Zhou, W. J.; Li, D. X.; Xiong, C. Y.; Yuan, R.; Xiang, Y. Multicolor-Encoded Reconfigurable DNA Nanostructures Enable Multiplexed Sensing of Intracellular MicroRNAs in Living Cells. *ACS Appl. Mater. Interfaces* **2016**, *8*, 13303-13308.
61. Li, N.; Wang, M. M.; Gao, X. N.; Yu, Z. Z.; Pan, W.; Wang, H. Y.; Tang, B. A DNA Tetrahedron Nanoprobe with Controlled Distance of Dyes for Multiple Detection in Living Cells and *in Vivo*. *Anal. Chem.* **2017**, *89*, 6670-6677.
62. Chandrasekaran, A. R.; Punnoose, J. A.; Zhou, L.; Dey, P.; Dey, B. K.; Halvorsen, K. DNA Nanotechnology Approaches for MicroRNA Detection and Diagnosis. *Nucleic Acids Res.* **2019**, *47*, 10489-10505.
63. He, L.; Lu, D.; Liang, H.; Xie, S.; Zhang, X.; Liu, Q.; Yuan, Q.; Tan, W. MRNA-Initiated, Three-Dimensional DNA Amplifier Able to Function inside Living Cells. *J. Am. Chem. Soc.* **2018**, *140*, 258-263.
64. Ma, Y.; Mao, G.; Huang, W.; Wu, G.; Yin, W.; Ji, X.; Deng, Z.; Cai, Z.; Zhang, X.-E.; He, Z.; Cui, Z. Quantum Dot Nanobeacons for Single RNA Labeling and Imaging. *J. Am. Chem. Soc.* **2019**, *141*, 13454-13458.
65. Liu, Y.; Le, P.; Lim, S. J.; Ma, L.; Sarkar, S.; Han, Z. Y.; Murphy, S. J.; Kosari, F.; Vasmatzis, G.; Chevillat, J. C.; Smith, A. M. Enhanced MRNA FISH with Compact Quantum Dots. *Nat. Commun.* **2018**, *9*, 4461.
66. Qu, A. H.; Sun, M. Z.; Xu, L. G.; Hao, C. L.; Wu, X. L.; Xu, C. L.; Kotov, N. A.; Kuang, H. Quantitative Zeptomolar Imaging of MiRNA Cancer Markers with Nanoparticle Assemblies. *Proc. Natl. Acad. Sci. U. S. A.* **2019**, *116*, 3391-3400.
67. Pan, W.; Liu, B.; Gao, X. N.; Yu, Z. Z.; Liu, X. H.; Li, N.; Tang, B. A Graphene-Based Fluorescent Nanoprobe for Simultaneous Monitoring of MiRNA and MRNA in Living Cells. *Nanoscale* **2018**, *10*, 14264-14271.
68. Dong, H.; Dai, W.; Ju, H.; Lu, H.; Wang, S.; Xu, L.; Zhou, S. F.; Zhang, Y.; Zhang, X. Multifunctional Poly(L-Lactide)-Polyethylene Glycol-Grafted Graphene Quantum Dots for Intracellular MicroRNA Imaging and Combined Specific-Gene-Targeting Agents Delivery for Improved Therapeutics. *ACS Appl. Mater. Interfaces* **2015**, *7*, 11015-11023.
69. Kim, E.; Yang, J.; Park, J.; Kim, S.; Kim, N. H.; Yook, J. I.; Suh, J.-S.; Haam, S.; Huh, Y.-M. Consecutive Targetable Smart Nanoprobe for Molecular Recognition of Cytoplasmic MicroRNA in Metastatic Breast Cancer. *ACS Nano* **2012**, *6*, 8525-8535.

70. Wang, Y.; Wu, C.; Chen, T.; Sun, H.; Cansiz, S.; Zhang, L.; Cui, C.; Hou, W.; Wu, Y.; Wan, S.; Cai, R.; Liu, Y.; Sumerlin, B. S.; Zhang, X.; Tan, W. DNA Micelle Flares: A Study of the Basic Properties That Contribute to Enhanced Stability and Binding Affinity in Complex Biological Systems. *Chem. Sci.* **2016**, *7*, 6041-6049.
71. Dong, X.; Ong, S. Y.; Zhang, C.; Chen, W.; Du, S.; Xiao, Q.; Gao, L.; Yao, S. Q. Broad-Spectrum Polymeric Nanoquencher as an Efficient Fluorescence Sensing Platform for Biomolecular Detection. *ACS Sens.* **2021**, *6*, 3102-3111.
72. Lin, L.-S.; Cong, Z.-X.; Cao, J.-B.; Ke, K.-M.; Peng, Q.-L.; Gao, J.; Yang, H.-H.; Liu, G.; Chen, X. Multifunctional Fe<sub>3</sub>O<sub>4</sub>@Polydopamine Core-Shell Nanocomposites for Intracellular mRNA Detection and Imaging-Guided Photothermal Therapy. *ACS Nano* **2014**, *8*, 3876-3883.
73. Sahay, G.; Alakhova, D. Y.; Kabanov, A. V. Endocytosis of Nanomedicines. *J. Control. Release* **2010**, *145*, 182-195.
74. Iversen, T. G.; Skotland, T.; Sandvig, K. Endocytosis and Intracellular Transport of Nanoparticles: Present Knowledge and Need for Future Studies. *Nano Today* **2011**, *6*, 176-185.
75. Patel, S.; Kim, J.; Herrera, M.; Mukherjee, A.; Kabanov, A. V.; Sahay, G. Brief Update on Endocytosis of Nanomedicines. *Adv. Drug Deliv. Rev.* **2019**, *144*, 90-111.
76. Ong, S. Y.; Zhang, C.; Xiao, D.; Yao, S. Q. Recent Advances in Polymeric Nanoparticles for Enhanced Fluorescence and Photoacoustic Imaging. *Angew. Chem. Int. Ed.* **2021**, *60*, 17797-17809.
77. Reisch, A.; Didier, P.; Richert, L.; Oncul, S.; Arntz, Y.; Mely, Y.; Klymchenko, A. S. Collective Fluorescence Switching of Counterion-Assembled Dyes in Polymer Nanoparticles. *Nat. Commun.* **2014**, *5*, 4089.
78. Reisch, A.; Trofymchuk, K.; Runser, A.; Fleith, G.; Rawiso, M.; Klymchenko, A. S. Tailoring Fluorescence Brightness and Switching of Nanoparticles through Dye Organization in the Polymer Matrix. *ACS Appl. Mater. Interfaces* **2017**, *9*, 43030-43042.
79. Reisch, A.; Runser, A.; Arntz, Y.; Mely, Y.; Klymchenko, A. S. Charge-Controlled Nanoprecipitation as a Modular Approach to Ultrasmall Polymer Nanocarriers: Making Bright and Stable Nanoparticles. *ACS Nano* **2015**, *9*, 5104-5116.
80. Reisch, A.; Heimburger, D.; Ernst, P.; Runser, A.; Didier, P.; Dujardin, D.; Klymchenko, A. S. Protein-Sized Dye-Loaded Polymer Nanoparticles for Free Particle Diffusion in Cytosol. *Adv. Funct. Mater.* **2018**, *28*, 1805157.
81. Andreiuk, B.; Reisch, A.; Lindecker, M.; Follain, G.; Peyrieras, N.; Goetz, J. G.; Klymchenko, A. S. Fluorescent Polymer Nanoparticles for Cell Barcoding *in Vitro* and *in Vivo*. *Small* **2017**, *13*, 1701582.
82. Trofymchuk, K.; Reisch, A.; Didier, P.; Fras, F.; Gilliot, P.; Mely, Y.; Klymchenko, A. S. Giant Light-Harvesting Nanoantenna for Single-Molecule Detection in Ambient Light. *Nat. Photonics* **2017**, *11*, 657.
83. Severi, C.; Melnychuk, N.; Klymchenko, A. S. Smartphone-Assisted Detection of Nucleic Acids by Light-Harvesting FRET-Based Nanoprobe. *Biosens. Bioelectron.* **2020**, *168*.
84. Egloff, S.; Melnychuk, N.; Reisch, A.; Martin, S.; Klymchenko, A. S. Enzyme-Free Amplified Detection of Cellular MicroRNA by Light-Harvesting Fluorescent Nanoparticle Probes. *Biosens. Bioelectron.* **2021**, *179*, 113084.
85. Melnychuk, N.; Ashokkumar, P.; Aparin, I. O.; Klymchenko, A. S. Pre- and Postfunctionalization of Dye-Loaded Polymeric Nanoparticles for Preparation of FRET-Based Nanoprobes. *ACS Appl. Mater. Interfaces* **2021**, DOI: 10.1021/acsapm.1c00819.
86. Andreiuk, B.; Reisch, A.; Bernhardt, E.; Klymchenko, A. S. Fighting Aggregation-Caused Quenching and Leakage of Dyes in Fluorescent Polymer Nanoparticles: Universal Role of Counterion. *Chem. Asian J.* **2019**, *14*, 836-846.
87. Olie, R. A.; Simões-Wüst, A. P.; Baumann, B.; Leech, S. H.; Fabbro, D.; Stahel, R. A.; Zangemeister-Wittke, U. A Novel Antisense Oligonucleotide Targeting Survivin Expression Induces Apoptosis and Sensitizes Lung Cancer Cells to Chemotherapy. *Cancer Res.* **2000**, *60*, 2805-2809.
88. Arvey, A.; Hermann, A.; Hsia, C. C.; Ie, E.; Freund, Y.; McGinnis, W. Minimizing Off-Target Signals in RNA Fluorescent *in Situ* Hybridization. *Nucleic Acids Res.* **2010**, *38*, e115.

89. Thomsen, R.; Nielsen, P. S.; Jensen, T. H. Dramatically Improved RNA *in Situ* Hybridization Signals Using LNA-Modified Probes. *RNA* **2005**, *11*, 1745-1748.
90. Floyd, D. L.; Ragains, J. R.; Skehel, J. J.; Harrison, S. C.; van Oijen, A. M. Single-Particle Kinetics of Influenza Virus Membrane Fusion. *Proc. Natl. Acad. Sci. U. S. A.* **2008**, *105*, 15382-15387.
91. Karstens, T.; Kobs, K. Rhodamine B and Rhodamine 101 as Reference Substances for Fluorescence Quantum Yield Measurements. *J. Phys. Chem.* **1980**, *84*, 1871-1872.
92. Texier, I.; Goutayer, M.; Da Silva, A.; Guyon, L.; Djaker, N.; Jossierand, V.; Neumann, E.; Bibette, J.; Vinet, F. Cyanine-Loaded Lipid Nanoparticles for Improved *in Vivo* Fluorescence Imaging. *J. Biomed. Opt.* **2009**, *14*, 054005.

## Table of contents graphic

